INSTITUTE OF PHYSICS PUBLISHING JOURNAL OF PHYSICS B: ATOMIC, MOLECULAR AND OPTICAL PHYSICS

J. Phys. B: At. Mol. Opt. Phys. **34** (2001) 4003–4013 PII: S0953-4075(01)26298-1

Electron-impact ionization of hydrogen-like iron ions

B O'Rourke[1,2], F J Currell[1,2], H Kuramoto[2], Y M Li[3], S Ohtani[2,3], X M Tong[2] and H Watanabe[2]

[1] Department of Physics, Queen's University Belfast, Belfast BT7 1NN, UK
[2] Cold Trapped Ions Project, ICORP, JST, Tokyo 182-0024, Japan
[3] University of Electro-Communications, Chofu, Tokyo 182-8585, Japan

E-mail: b.orourke@qub.ac.uk

Received 2 July 2001, in final form 23 August 2001
Published 5 October 2001
Online at stacks.iop.org/JPhysB/34/4003

Abstract

Electron-impact ionization cross sections have been determined for hydrogen-like iron ions at selected electron energies between 1.45 and 4.3 times the threshold energy. The cross sections were obtained by measuring the equilibrium ionization balance in an electron beam ion trap. This ionization balance is obtained from x-ray measurements of radiative recombination into the K-shell of hydrogen-like and bare iron ions. The measured cross sections are compared with distorted-wave calculations and several semiempirical formulations.

1. Introduction

Electron-impact ionization of hydrogen-like ions is the process by which an incident electron removes the final bound electron from an ion leaving a bare nucleus. All effects due to the presence of other bound electrons are absent, only direct ionization contributes to the cross section. Effects such as excitation autoionization or resonant processes do not occur.

High-Z hydrogen-like ions may occur in high-temperature plasmas such as astrophysical or fusion plasmas. Iron is an important constituent of astrophysical plasmas with charge states of up to Fe^{25+}, having been observed in violent solar events such as solar flares (Pike *et al* 1996) and from x-ray observations of the Seyfert galaxy Markarian 3 (Sako *et al* 2000). Accurate cross sections for the atomic processes occurring in these plasmas are needed as inputs for ionization models.

Absolute ionization cross sections for low-charge-state hydrogen-like ions have been obtained by the crossed-beams technique (Aichele *et al* 1998), and by modelling the measured charge-state evolution of ions in an electron beam ion source (EBIS) (Donets and Ovsyannikov 1981). For high-Z ions several species have been measured in the Livermore electron beam ion trap (EBIT) (Marrs *et al* 1994, 1997). However, no measurements exist in the intermediate-Z range including Fe^{25+}, the subject of this paper.

Measurements in this Z region are also important from a theoretical point of view. For low-Z ions classical theory may be used to describe the ionization processes and semiempirical formula such as that due to Lotz (1968) can be used. For high-Z ions a relativistic theory must be used and contributions from quantum electrodynamics (QED) effects become important as the charge state is increased.

2. Experimental method

Ionization cross sections of hydrogen-like ions have been measured previously using an EBIT (Marrs *et al* 1994, 1997). The method used in the present study is an extension of the method used in those experiments, where a comparison of the number of trapped hydrogen-like and bare ions, together with a correction for charge exchange, was used to determine the hydrogen-like ionization cross section.

2.1. Method

Hydrogen-like and bare iron ions were trapped in the Tokyo EBIT (Currell *et al* 1996). Low-charge-state iron ions were introduced to the trap region and rapidly ionized by the electron beam. The trap is composed of three coaxial cylindrical electrodes or drift tubes, DT1, DT2 and DT3. The ions were trapped in DT2, axially by the potentials applied to DT1 and DT3 and radially by the space charge of the electron beam.

Iron ions of low-charge state were injected into the Tokyo EBIT using a metal vacuum vapour arc source (MEVVA) (Brown *et al* 1986). When the MEVVA was fired low-charge-state iron ions were produced and were accelerated along the beam axis towards the trap. The potential of DT3 was then lowered and quickly raised again in order to capture some ions in the trap. Once the ions are trapped, the electron beam strips the outer electrons by successive impact ionization and the hydrogen-like stage is reached very quickly, typically after less than 0.5 s depending on the electron beam energy and current.

In order to increase the trapping time of the highly charged ions a beam of neutral neon atoms was injected into the trap region at 90° to the electron beam. Some of these atoms are ionized by the beam or by charge exchange and are captured in the trap. Ion–ion collisions between these low-charge-state neon ions and the highly charged ions transfer energy to the neon ions which may subsequently escape from the trap with the removal of energy (Schneider *et al* 1989).

After the MEVVA was triggered and ions were trapped, x-rays were detected for a 4 s period. The DT3 potential was then lowered and the trap emptied. This was to avoid build up of unwanted barium ions which are removed from the cathode and accrete in the trap. Also the highly charged iron ions are gradually lost and so it is necessary to periodically dump and refill the trap. Using the multiparameter system described previously (Currell *et al* 1997) both the x-ray energy and the time during the cycle at which it is detected were recorded and a two-dimensional map produced.

X-rays from radiative recombination (RR) were detected at 90° to the electron beam by a Si(Li) solid-state detector. RR lines from K-shell capture were used to infer the ionization balance of hydrogen-like and bare ions. From this balance the electron-impact ionization cross section can be determined after a correction for charge exchange has been taken into account.

2.2. Equilibrium analysis

The rate of change of the number of trapped bare ions can be written as

$$\frac{\mathrm{d}N_\mathrm{B}}{\mathrm{d}t} = -\left(\frac{J}{e}\right) N_\mathrm{B} f_\mathrm{B} \sigma_\mathrm{B}^{\sum \mathrm{RR}} + \left(\frac{J}{e}\right) N_\mathrm{H} f_\mathrm{H} \sigma_\mathrm{H}^{\mathrm{EI}} - N_0 N_\mathrm{B} \left\langle \sigma_\mathrm{B}^{\mathrm{CX}} \right\rangle \tag{1}$$

where N_B and N_H are the numbers of bare and hydrogen-like ions, J is the electron beam current density, f_B and f_H the overlap factors of the ion clouds with the electron beam and N_0 the number of neutral atoms. $\sigma^{\sum \mathrm{RR}}$, σ^{EI} and $\langle \sigma^{\mathrm{CX}} \rangle$ are the total radiative recombination, the electron-impact ionization and the effective charge-exchange cross sections, respectively.

After equilibrium has been reached, $\frac{\mathrm{d}N_\mathrm{B}}{\mathrm{d}t} = 0$, and we can write,

$$\sigma_\mathrm{H}^{\mathrm{EI}} = \frac{N_\mathrm{B} f_\mathrm{B} \sigma_\mathrm{B}^{\sum \mathrm{RR}}}{N_\mathrm{H} f_\mathrm{H}} + \frac{N_0 N_\mathrm{B} \left\langle \sigma_\mathrm{B}^{\mathrm{CX}} \right\rangle}{N_\mathrm{H} f_\mathrm{H} \left(J/e\right)}. \tag{2}$$

We can relate N_B and N_H to the yield of RR x-ray photons due to capture into $n = 1$ observed at 90° into solid angle Ω, using the relations,

$$N_{h\nu_\mathrm{B}} = \frac{I_\mathrm{e}}{r_\mathrm{b}^2} N_\mathrm{B} \frac{\mathrm{d}\sigma_\mathrm{B}^{\mathrm{RR}=1}}{\mathrm{d}\Omega} \mathrm{d}\Omega \tag{3}$$

$$N_{h\nu_\mathrm{H}} = \frac{I_\mathrm{e}}{r_\mathrm{b}^2} N_\mathrm{H} \frac{\mathrm{d}\sigma_\mathrm{H}^{\mathrm{RR}=1}}{\mathrm{d}\Omega} \mathrm{d}\Omega \tag{4}$$

where $N_{h\nu\mathrm{B}}$ and $N_{h\nu\mathrm{H}}$ are the respective photon yields as measured by the detector, I_e is the electron beam current, r_b is the beam radius and $\mathrm{d}\sigma_\mathrm{B}^{\mathrm{RR}=1}/\mathrm{d}\Omega$, $\mathrm{d}\sigma_\mathrm{H}^{\mathrm{RR}=1}/\mathrm{d}\Omega$ are the differential $n = 1$ RR cross sections at 90°. The beam radius has been shown to be weakly dependent on the current (Kuramoto *et al* 2001). For the beam energies, currents and axial trapping depth under consideration the overlap factors f_B and f_H are approximately equal with values close to 1. Equation (2) can then be written as

$$\sigma_\mathrm{H}^{\mathrm{EI}} = \frac{N_{h\nu\mathrm{B}}}{N_{h\nu\mathrm{H}}} \frac{\sigma_\mathrm{B}^{\sum \mathrm{RR}} \left(\mathrm{d}\sigma_\mathrm{H}^{\mathrm{RR}=1}/\mathrm{d}\Omega\right)}{\left(\mathrm{d}\sigma_\mathrm{B}^{\mathrm{RR}=1}/\mathrm{d}\Omega\right)} \left(1 + \frac{N_0}{I} \left\langle \sigma_\mathrm{B}^{\mathrm{CX}} \right\rangle_{\mathrm{eff}}\right) \tag{5}$$

where $\langle \sigma_\mathrm{B}^{\mathrm{CX}} \rangle_{\mathrm{eff}}$ is an effective charge-exchange cross section given by,

$$\left\langle \sigma_\mathrm{B}^{\mathrm{CX}} \right\rangle_{\mathrm{eff}} = \frac{r_\mathrm{b}^2}{\sigma_\mathrm{B}^{\sum \mathrm{RR}}} \left\langle \sigma_\mathrm{B}^{\mathrm{CX}} \right\rangle. \tag{6}$$

All relevant RR cross sections were calculated theoretically to high accuracy (section 2.3). The effective charge-exchange contribution is therefore the only unknown factor in equation (5). To take account of this we have performed the experiment at various neutral gas densities, N_0, and beam currents, I.

2.3. Theoretical calculations

Radiative recombination cross sections can be obtained by applying the detailed balance to the photoionization cross sections (Ichihara *et al* 1994) as (in atomic units with $\hbar = m = e = 1$)

$$\frac{\mathrm{d}\sigma_{\mathrm{RR}}}{\mathrm{d}\Omega} = \frac{(1 - f_i)\left(\gamma - 1 + E_\mathrm{b}/c^2\right)^2}{\gamma^2 - 1} \frac{\mathrm{d}\sigma_\mathrm{p}}{\mathrm{d}\Omega} \tag{7}$$

with $\gamma = E_e/c^2 + 1$. E_e and E_b are the electron beam energy and binding energy of the final bound state. The emitted photon has energy $E_e + E_b$. The occupation coefficient f_i is defined as $f_i = N_c/(2j+1)$, with j the final-state total angular momentum. The differential photoionization cross section can be expressed as

$$\frac{d\sigma_p}{d\Omega} = \frac{\sigma_{total}}{4\pi}\left[\sum_{l=0}^{l_{max}} B_1(l)\,P_1(\cos\theta) + \sum_{l=2}^{l_{max}} B_2(l)\,P_l^2(\cos\theta)\cos(2\phi)\right]. \tag{8}$$

The total cross section and the angular distribution coefficients can be calculated for a given effective potential based on the independent particle approximation (IPA) (Tseng *et al* 1978, Kim *et al* 1980, Scofield 1989). The effective potential obtained from relativistic density functional theory with an optimized effective potential and self-interaction correction method was used (Tong and Chu 1998). This is more accurate than the popular relativistic self-consistent potential method (Liberman *et al* 1971).

To calculate the total RR cross section, $\sigma_B^{\sum RR}$, the sum of all the RR cross sections to any excited state must be obtained. To do this we first calculate the cross sections for $n = 1$, 2, 3, 4 with all possible partial waves. Then since the normalization of a given wavefunction in the inner region is scaled by n^3, the RR cross section for highly excited ions can be scaled by $1/n^3$. Thus the total RR cross section can be expressed as

$$\sigma_{total}^{RR} = \sum_j \left\{\sum_{i=1}^{3}\sigma_{i,j}^{RR} + 64\sigma_{4,j}^{RR}\left[\sum_{n=4}^{\infty}\frac{1}{n^3}\right]\right\}. \tag{9}$$

By comparing scaled calculated RR cross sections, the validity of the n^3 scaling was seen to be accurate to within a few per cent, so equation (9) can be used to obtain a converged total RR cross section.

One further point to note is that the ratio of differential cross sections for radiative recombination into bare and hydrogen-like ions,

$$\frac{d\sigma_B^{RR=1}/d\Omega}{d\sigma_H^{RR=1}/d\Omega}$$

was calculated explicitly. For highly charged ions a value of 2.0 has been assumed previously by Marrs *et al* (1997). For the electron energies under consideration in this experiment the value is between 2.044 and 2.024 (table 2).

3. Results

A typical x-ray spectrum at 15 keV is shown in figure 1. The x-ray energy scale was calibrated from reference peaks in the decay spectra of ^{241}Am and ^{57}Co. The highest-energy x-ray peak is a barely resolved doublet, which corresponds to RR into the K shell of hydrogen-like and bare iron ions. At these energies there is a small contribution due to RR into the L shell of highly charged barium ions, which must be taken into account.

The blend of ionization states contributing to this broad peak was found to be helium-like to boron-like barium ions. The ionization energies of lithium to carbon-like barium ions along with the both helium-like and hydrogen-like iron ions are shown in table 1. Energy levels for the barium ions were obtained using the GRASP code (Dyall *et al* 1989), a fully relativistic atomic structure code. The iron ionization energies were taken from data tables, for hydrogen-like iron Johnson and Soff (1985) and for helium-like iron from Drake (1988).

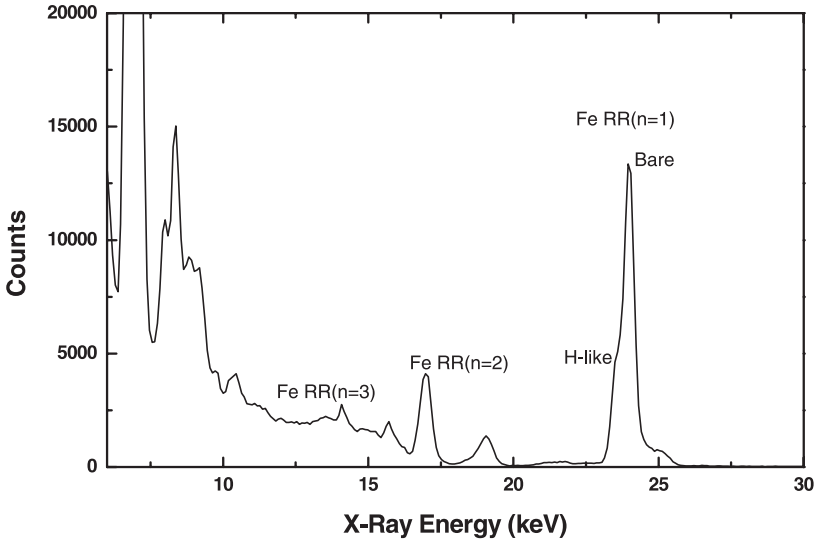

Figure 1. Typical x-ray spectrum obtained at an electron energy of 15 keV. Beyond the electron energy a series of peaks can be seen which correspond to radiative recombination into low-lying levels of very highly charged iron ions. The peak at the highest energy is due to RR into the $n = 1$ level of hydrogen-like and bare ions.

Table 1. Ionization potentials for various charge states of Ba and Fe ions.

Element	Ionization stage	IP (keV)
Barium	Li	10.621
	Be	10.377
	B	10.023
	C	9.738
Iron	H	9.278
	He	8.828

The x-ray spectra were then fitted with six Gaussians, corresponding to the four barium states and two iron states, the energy separation between the peaks being fixed according to table 1. The fitting procedure had nine free parameters, the heights of the six peaks, a peak width (assumed to be the same for each peak), a small constant background and one variable describing the position of the peaks, from which the electron energy is deduced. The heights of the hydrogen-like and bare peaks were used to infer the relative abundances of these ions.

The fitting function used is represented by the following expression (with all fitting parameters in italics):

$$\text{fitting function} = A_{\mathrm{H}} \exp\left[-\frac{(\mathrm{x} - x_{\mathrm{B}} + \mathrm{d_H})^2}{\sigma}\right] + A_{\mathrm{B}} \exp\left[-\frac{(\mathrm{x} - x_{\mathrm{B}})^2}{\sigma}\right] + \sum_{i=1}^{4} A_i \exp\left[-\frac{(\mathrm{x} - x_{\mathrm{B}} + \mathrm{d}_i)^2}{\sigma}\right] + \text{constant} \tag{10}$$

where A_{H} and A_{B} are the amplitude of the hydrogen-like and bare peaks, x_{B} is the position of the bare peak and $\mathrm{d_H}$ is the fixed separation between this and the hydrogen-like peak. The barium contribution is represented by the sum of four Gaussian profiles each with a peak height

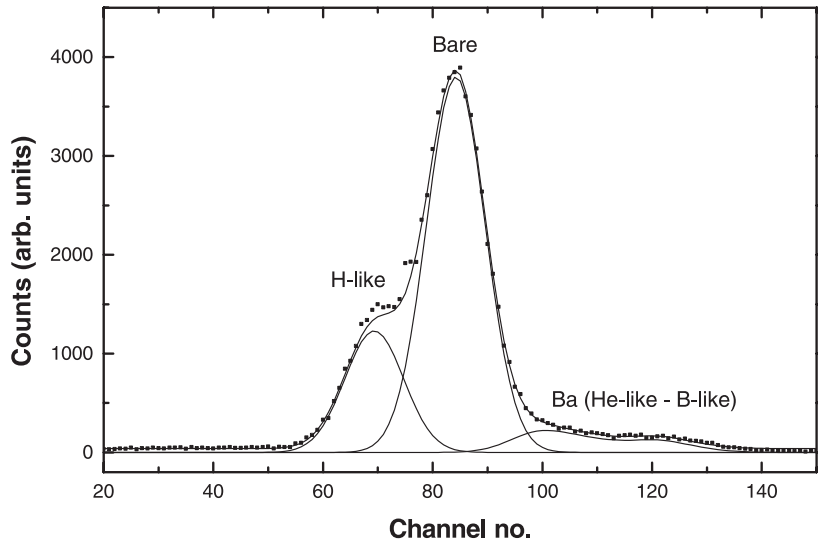

Figure 2. A typical fit to the RR ($n = 1$) x-ray spectra. The hydrogen-like and bare components are shown along with a blend of four barium states. The sum of these components is also plotted and can be seen to follow the measured data very closely.

A_i and a fixed separation from the bare peak, d_i. A typical fit at 15 keV is shown in figure 2. The individual contributions from hydrogen-like and bare iron and the barium blend are plotted along with their sum.

3.1. Equilibrium

As was mentioned earlier the analysis is only valid when the system is in equilibrium, i.e. when the relative populations of hydrogen-like and bare ions remains constant. In order to ensure that this was the case the x-ray spectrum was fitted at various times throughout the cycle. The 4096 time channels recorded by the multiparameter system were compressed 100-fold to create 40 separate time channels. Each of these was fitted using the procedure outlined above and the ratio of hydrogen-like to bare ions calculated in each case. The range of times over which this ratio was constant was noted and only data collected within this time window used for further analysis. Ten separate spectra were then created from this reduced dataset. These spectra were created by taking each tenth event in this reduced dataset. The ten new spectra were each fitted again with the procedure outlined above. These spectra were then statistically independent and performing individual fits to them is equivalent to performing the experiment ten times. From these fits an average value and a standard deviation were obtained and used to calculate the cross section and the statistical error.

3.2. Charge-exchange correction

In order to account for charge exchange the experiment was performed over a range of neutral densities and beam currents. Initially the electron beam energy was held at 15 keV and the current at 160 mA and the neutral density was varied. We assume that the neutral neon density is proportional to the pressure measured at the final stage of the injector. The actual neutral density in the trap is much lower than indicated by this pressure reading.

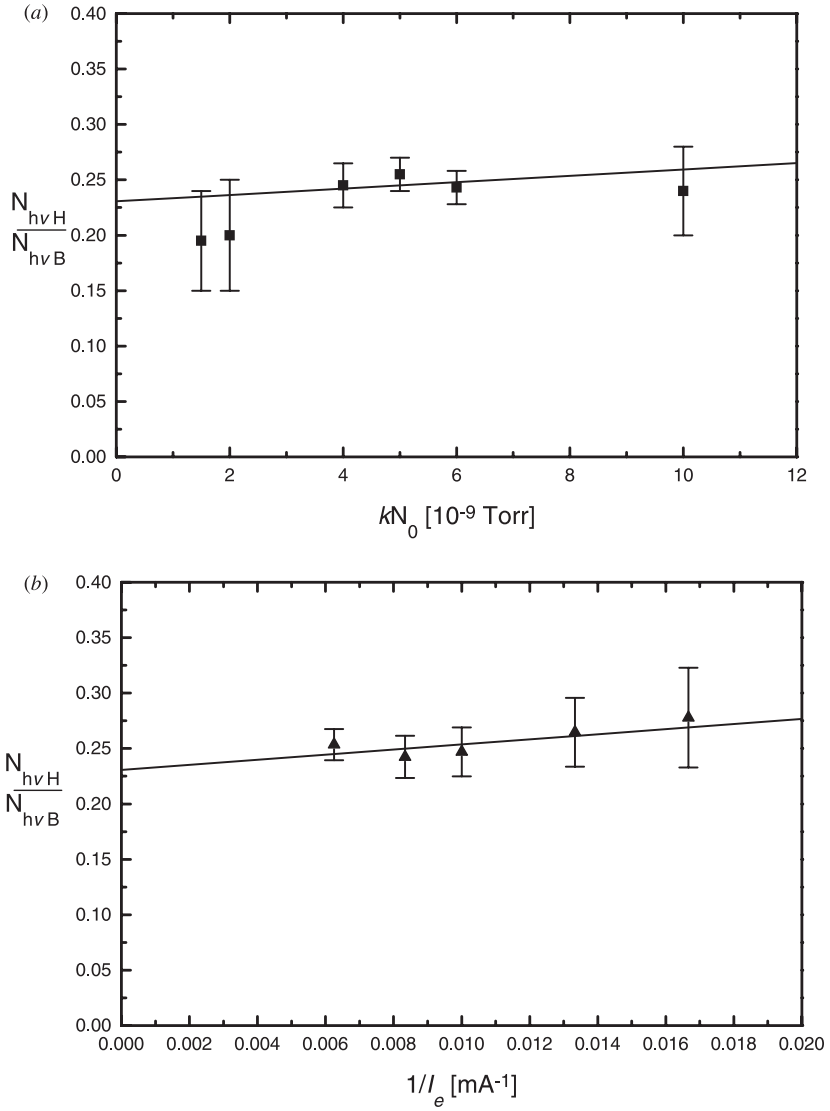

Figure 3. The measured population balance of hydrogen-like and bare ions at 15 keV as a function of (*a*) gas injector pressure and (*b*) the electron current. A simultaneous fit of this complete data set gave the fit shown in both graphs. The intercept on the y-axis (the same in both cases) gives the cross section at 15 keV, while the slope gives the charge-exchange contribution.

The beam current was then varied, holding the neutral density fixed at an injector pressure of 5×10^{-9} Torr and the beam energy at 15 keV. The results from both of these experiments were then fitted to equation (5), with N_0 and I as variables. The results of this fit are shown in figure 3. The intercept on the y-axis gives the corrected cross section at 15 keV, while the slope indicates the charge-exchange contribution. An error in the slope is obtained from the fitting procedure and corresponds to the error in the charge-exchange correction. The error in the cross section is then a sum of the statistical error and the error in the charge-exchange correction.

Measurements were then taken at various electron beam energies from 13.5 to 40 keV with a beam current of 160 mA and a neutral density of 5×10^{-9} Torr in each case. The spectra were fitted using the procedure outlined and the uncorrected cross sections and statistical errors calculated. The effective charge-exchange contribution and associated error were then included and the corrected ionization cross sections calculated. From the fitting procedure outlined above the absolute energy of the hydrogen-like and bare x-ray peaks can be obtained. Using the ionization potentials quoted in table 1 this allows us to determine the electron beam energy. The experiment was performed at 13.5, 15, 17.5, 20, 25, 30 and 40 keV as determined by the power supply values. However, the space charge of the electron beam lowers the potential at the centre of the trap according to the formula (Currell 2000)

$$V_{\mathrm{sp}} = \left(2 \ln \frac{r_{\mathrm{dt}}}{r_{\mathrm{b}}} + 1\right) \frac{30 I[\mathrm{A}]}{\sqrt{1 - (Ee[\mathrm{keV}]/511 + 1)^{-2}}} \tag{11}$$

where r_{dt} is the drift tube radius which is 5 mm for the Tokyo EBIT. For a beam radius of 50 μm, an electron beam energy of 15 keV and a beam current of 160 mA the potential shift is estimated to be 207 V. Therefore, the electron energy as seen by the ions is lower than the accelerating potential applied to the power supplies and we use the value obtained through the fitting procedure which is some 200–250 V lower than the 'actual' electron energy, providing confirmation of the electron beam radius.

Table 2. Ionization cross sections for hydrogen-like iron ions. Calculated radiative recombination differential and total cross sections as explained in the text are shown (differential in units of 10^{-24} cm^2/Sr and total in units of 10^{-24} cm^2). The final column gives the ionization cross sections and associated errors in units of 10^{-22} cm^2.

Electron energy (keV)	$\frac{\mathrm{d}\sigma_{\mathrm{B}}^{\mathrm{RR}=1}}{\mathrm{d}\Omega}$	$\frac{\mathrm{d}\sigma_{\mathrm{H}}^{\mathrm{RR}=1}}{\mathrm{d}\Omega}$	$\frac{\mathrm{d}\sigma_{\mathrm{B}}^{\mathrm{RR}=1}/\mathrm{d}\Omega}{\mathrm{d}\sigma_{\mathrm{H}}^{\mathrm{RR}=1}/\mathrm{d}\Omega}$	$\sigma_{\mathrm{B}}^{\sum \mathrm{RR}}$	$\frac{N_{h\upsilon \mathrm{B}}}{N_{h\upsilon \mathrm{H}}}$	$\sigma_{\mathrm{H}}^{\mathrm{EI}}$
13.3	6.199	3.033	2.044	77.32	2.410	0.93 ± 0.24
14.8	5.185	2.539	2.042	64.81	3.953	1.30 ± 0.12
17.3	3.951	1.937	2.040	49.73	5.848	1.51 ± 0.15
19.8	3.115	1.529	2.037	39.58	8.065	1.69 ± 0.23
24.8	2.050	1.008	2.034	26.67	11.76	1.75 ± 0.34
29.8	1.434	0.7063	2.030	19.18	18.52	2.08 ± 0.79
39.6	0.7934	0.3919	2.024	11.28	27.78	2.12 ± 1.18

The measured electron-impact ionization cross sections and associated errors are shown in table 2. At high energies the errors grow due to the fact that the radiative recombination cross section decreases and the statistics become poorer. As the energy is reduced towards the ionization potential the ionization cross section is reduced and the number of bare and hydrogen-like ions decrease. Again the statistics become poorer and the barium contamination becomes a barrier to more accurate measurements.

4. Discussion

The measured ionization cross sections for hydrogen-like iron are plotted in figure 4. Several theoretical plots have also been included for comparison. We have performed our own theoretical analysis for this process. A distorted-wave method was used, with parameters and wavefunctions of bound states obtained from calculations using the GRASP code (Dyall *et al* 1989). The calculation does not include the Breit and Møller interactions. For hydrogen-

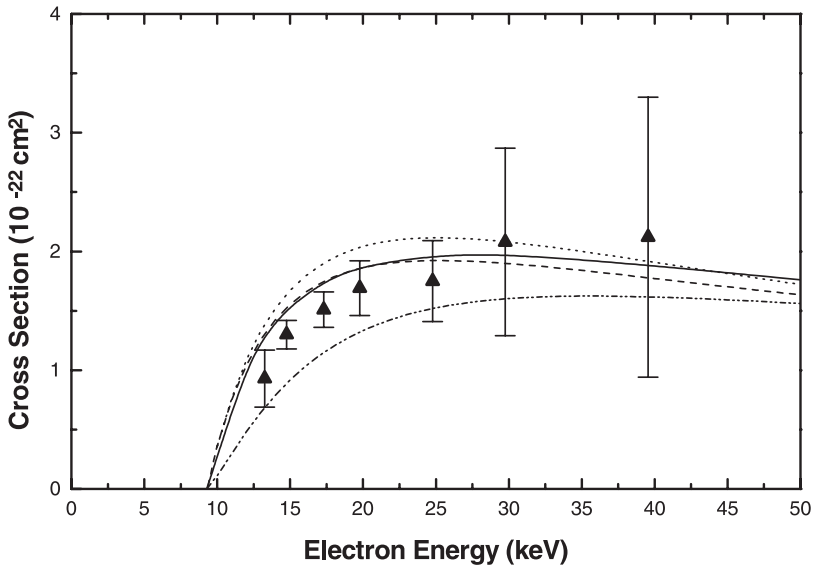

Figure 4. The measured ionization cross sections for hydrogen-like iron along with our theoretical calculation based on a distorted-wave method (——). Also included are the semiempirical Lotz formula (– – –), the universal shape parametrization due to Aichele *et al* (1998) (· · · · · ·) and the treatment due to Deutsch *et al* (1995) (— · —).

like iron, however, the contribution from these interactions was estimated to be 1–2%. This calculation is plotted as a full curve in figure 4.

A semiempirical formula due to Lotz (1967, 1968) can be used to predict electron-impact ionization cross sections. For hydrogen-like ions it has the form

$$\sigma_{\mathrm{H}}^{\mathrm{EI}} = a_i \frac{\ln\left(E_{\mathrm{e}}/I_{\mathrm{H}}\right)}{E_{\mathrm{e}} I_{\mathrm{H}}}, \qquad a_i = 4.5 \times 10^{-14}\ \mathrm{cm}^2\ (\mathrm{eV})^2 \tag{12}$$

where E_{e} is the incident electron energy and I_{H} is the ionization potential of the hydrogen-like ion. The curve obtained using this formula is shown as a broken curve in figure 4.

A second semiempirical formula derived more recently is also shown. A scaling for obtaining a universal shape function of the ionization cross section was derived (Rost and Pattard 1997, Aichele *et al* 1998). The shape function is scaled by the maximum value σ_{M} of the cross section and the excess energy above threshold E_{M} where this maximum occurs. The analytical form which describes the universal shape is given by

$$\sigma(x) = \sigma_{\mathrm{M}} \left[\cosh\left(\beta \ln x\right)\right]^{-1/\beta} \tag{13}$$

where $x = (E - I)/E_{\mathrm{M}}$, and the power β was determined to be equal to 0.4 to provide the correct fit to the experimental data for ionization of low-charge-state hydrogen-like ions.

This analysis was extended (Aichele *et al* 1998) to provide scaling functions along the hydrogen-like isoelectronic sequence. The scales $\sigma_{\mathrm{M}} = \sigma_{\mathrm{M}}(Z)$ and $E_{\mathrm{M}} = E_{\mathrm{M}}(Z)$ were expressed as a function of Z using the available experimental data. The functions are given by

$$E_{\mathrm{M}}(Z) = I_{\mathrm{Hyd}} \left(3.31 + 5.07(Z-1) + 1.65(Z-1)^2\right) \tag{14}$$

$$\sigma_{\mathrm{M}}(Z) = \pi a_0^2 \left(\frac{1.0278}{1.0975 + Z - 1}\right)^4 \tag{15}$$

in units of the binding energy $I_{\mathrm{Hyd}} = 13.6$ eV of hydrogen and the Bohr radius a_0. Using these equations a prediction for the hydrogen-like ionization cross section of iron was obtained and is plotted in figure 4.

Absolute and scaled electron-impact ionization cross sections for hydrogen-like ions were calculated by Deutsch *et al* (1995). They used the semiclassical Deutsch–Märk (DM) approach (Deutsch and Märk 1987) which is based on a combination of the classical binary-encounter approximation and the Born–Bethe approximation. The formula obtained using this method is given as a function of U, where $U = E_{\mathrm{e}}/I_{\mathrm{H}}$, the electron energy divided by the ionization potential,

$$\sigma Z^{4.155} = 5.08 \times 10^{-16} f(U) F(U) \tag{16}$$

where $f(U)$ is given by

$$f(U) = U^{-1}\left[(U-1)/(U+1)\right]^{a}\left\{b + c\left[1-(2U)^{-1}\right]\ln\left[2.7+(U-1)^{0.5}\right]\right\} \tag{17}$$

and the parameters $a = 1.30, b = 0.75, c = 0.68$ were found empirically. $F(U)$ is a relativistic factor given by

$$F(U) = R(U)\left[1+(2U)^{0.25}/J^2\right] \tag{18}$$

and

$$R(U) = \left[\frac{1+2J}{U+2J}\right]\left[\frac{U+J}{1+J}\right]^2\left[\frac{(1+U)(U+2J)(1+J)^2}{J^2(1+2J)+U(U+2J)(1+J)^2}\right]^{1.5} \tag{19}$$

where $J = (m_{\mathrm{e}}c^2)/I_{\mathrm{H}}$. The cross section as predicted by this method is also plotted in figure 4.

The experimental results are in good general agreement with the various theoretical approaches. The distorted-wave calculation, which is the most rigorous, overestimates the measured cross section at low energies. This trend is also observed for both the Lotz and Rost–Pattard approaches. The semiclassical DM calculation, however, underestimates the measured values. The error in the measurement makes it impossible to differentiate between the various theoretical methods considered. The fact that the Lotz equation agrees well with the distorted-wave calculation suggests that relativistic effects are not very important in this system, at least up to several times the threshold energy.

5. Conclusion

We have measured electron-impact ionization cross sections of hydrogen-like iron at selected energies between 13.5 and 40 keV, 1.45–4.3 times threshold. Previously no measurements of this type had been preformed in the charge range O^{7+} to Mo^{41+}. The measurements have been compared with a relativistic distorted-wave calculation and several non-relativistic semiempirical formulations. For the electron-impact ionization of Fe^{25+} relativistic effects are assumed to be small but non-negligible. Our measurements are not of sufficient accuracy to discern between the relevant theoretical calculations. Accurate measurements of electron-impact ionization cross sections of other highly charged ions are needed to help guide our current understanding of this process.

Acknowledgments

This work was performed under the auspices of the International Cooperative Research Project (ICORP) of the Japan Science and Technology Corporation. Mobility support from the Sasakawa foundation and the Royal Society is gratefully acknowledged and BO'R is indebted to the Department of Education, Northern Ireland for the award of a postgraduate studentship.

References

Aichele K, Hartenfeller U, Hathiramani D, Hofmann G, Schafer V, Steidl M, Stenke M, Salzborn E, Pattard T and Rost J M 1998 *J. Phys. B: At. Mol. Opt. Phys.* **31** 2369

Brown I G, Galvin J E, MacGill R A and Wright R T 1986 *Appl. Phys. Lett.* **49** 1019

Currell F J 2000 *The Physics of Electron Beam Ion Traps, Trapping Highly Charged Ions: Fundamentals and Applications* ed J Gillaspy (New York: Nova)

Currell F J *et al* 1996 *J. Phys. Soc. Japan* **65** 3186

——1997 *Phys. Scr.* T **73** 371

Deutsch H, Becker K and Märk T D 1995 *Int. J. Mass Spectrom. Ion Proc.* **151** 207

Deutsch H and Märk T D 1987 *Int. J. Mass Spectrom. Ion Proc.* **79** R1

Donets E D and Ovsyannikov V P 1981 *Zh. Eksp. Teor. Fiz.* **80** 916 (Engl. transl. 1981 *Sov. Phys.–JETP* **53** 466)

Drake G W 1988 *Can. J. Phys.* **66** 586

Dyall K G, Grant I P, Jhonson C T, Parpia F A and Plummer E P 1989 *Comput. Phys. Commun.* **55** 425

Ichihara A, Shirai T and Eichler J 1994 *Phys. Rev.* A **49** 1875

Johnson W R and Soff G 1985 *At. Data Nucl. Data Tables* **33** 405

Kim Y S, Pratt R H, Ron A and Tseng H K 1980 *Phys. Rev.* A **22** 567

Kuramoto H, Watanabe H and Yamada I 2001 *Rev. Sci. Instrum.* submitted

Liberman D A, Cromer D T and Waber J T 1971 *Comput. Phys. Commum.* **2** 107

Lotz W 1967 *Astrophys. J. Suppl.* **14** 207

——1968 *Z. Phys.* **216** 241

Marrs R E, Elliott S R and Knapp D A 1994 *Phys. Rev. Lett.* **72** 4082

Marrs R E, Elliott S R and Scofield J H 1997 *Phys. Rev.* A **56** 1338

Pike C D, Phillips K J H, Lang J, Sterling A, Watanabe T, Hiei E, Culhane J L, Cornille M and Dubau U 1996 *Astrophys. J.* **464** 487

Rost J M and Pattard T 1997 *Phys. Rev.* A **55** R5

Sako M, Kahn S M, Paerels F and Liedahl D A 2000 *Astrophys. J. Lett.* **543** L115

Schneider M B, Levine M A, Bennett C L, Henderson J R, Knapp D A and Marrs R E 1989 *Int. Symp. on Electron Beam Ion Sources and their Applications (AIP Conf. Proc. no 188)* ed A Hershcovitch (New York: AIP) p 158

Scofield J H 1989 *Phys. Rev.* A **40** 3045

Tong X M and Chu S I 1998 *Phys. Rev.* A **57** 855

Tseng H K, Pratt R H, Yu S and Ron A 1978 *Phys. Rev.* A **17** 1061